

Accepted Article

Title: Linkage effect in the heterogenization of cobalt complexes by doped graphene for electrocatalytic CO₂ reduction

Authors: Xin Wang, Jiong Wang, Xiang Huang, Shibo Xi, Jong-Min Lee, Cheng Wang, and Yonghua Du

This manuscript has been accepted after peer review and appears as an Accepted Article online prior to editing, proofing, and formal publication of the final Version of Record (VoR). This work is currently citable by using the Digital Object Identifier (DOI) given below. The VoR will be published online in Early View as soon as possible and may be different to this Accepted Article as a result of editing. Readers should obtain the VoR from the journal website shown below when it is published to ensure accuracy of information. The authors are responsible for the content of this Accepted Article.

To be cited as: *Angew. Chem. Int. Ed.* 10.1002/anie.201906475
Angew. Chem. 10.1002/ange.201906475

Link to VoR: <http://dx.doi.org/10.1002/anie.201906475>
<http://dx.doi.org/10.1002/ange.201906475>

Linkage effect in the heterogenization of cobalt complexes by doped graphene for electrocatalytic CO₂ reduction

Jiong Wang,^{‡#} Xiang Huang,^{Δ#} Shibo Xi,[§] Jong-Min Lee,[‡] Cheng Wang,[&] Yonghua Du,^{§1} Xin Wang^{‡*}

[‡]School of Chemical and Biomedical Engineering, Nanyang Technological University, 62 Nanyang Drive, Singapore 639798, Singapore

^ΔDepartment of Physics, Southern University of Science and Technology, Shenzhen 518055, China.

[&]Institute for New Energy Materials & Low-Carbon Technologies, Tianjin University of Technology, Tianjin, 300384, P.R. China

[§]Institute of Chemical and Engineering Sciences, Agency for Science, Technology and Research (A*STAR), Singapore 627833, Singapore

¹Present address: National Synchrotron Light Source II, Brookhaven National Laboratory Upton NY, 11973 USA

*E-mail: WangXin@ntu.edu.sg

Abstract

Immobilization of planar Co(II)-2,3-naphthalocyanine (NapCo) complexes onto doped graphene resulted in a heterogeneous molecular Co electrocatalyst that was active and selective to reduce CO₂ into CO in aqueous solution. A systematic study revealed that graphitic sulfoxide and carboxyl dopants of graphene were the efficient binding sites for the immobilization of NapCo through axial coordination and resulted in active Co sites for CO₂ reduction. Compared to carboxyl dopants, the sulfoxide dopants further improved the electron communication between NapCo and graphene, which led to the increase of turnover frequency of Co sites by ~ 3 times for CO production with a Faradic efficiency up to 97%. Pristine NapCo in the absence of graphene supports did not display efficient electron communication with electrode and thus failed to serve as the electrochemical active sites for CO₂ reduction under the identical conditions.

Introduction

Conversion of carbon dioxide (CO₂) into fuels or chemicals is a potential solution to reduce our dependence on fossil fuels and address the environmental issues arising from

the use of such fuels. Of particular interest is electrochemical CO₂ reduction, which can sustainably convert CO₂ into carbonaceous fuels at mild conditions through the electrical inputs from renewable energies.^[1] CO₂ reduction reaction (CO₂RR) is a challenging task because CO₂ is chemically inert and the conversion needs to compete with hydrogen evolution if it is conducted in aqueous solution. The process is also complicated that involves multiple protons coupled electron transfer steps leading to various products.^[2] As a main and profitable product of CO₂RR, carbon monoxide (CO) can be used in syngas for production of hydrocarbons and their oxygenated derivatives via the Fischer-Tropsch process.^[3] Both homogeneous and heterogeneous catalysts have been explored for the selective production of CO. In principle, homogeneous catalysts, such as metal complexes and organometallic compounds, contain molecularly uniform and well-defined active sites that can be tuned systematically to achieve high selectivity and turnover frequencies (TOFs).^[4] Furthermore, they can be an ideal platform to probe the mechanism of CO₂RR at molecular levels and guide the rational design of catalysts.^[5] However, homogeneous catalysts often need aprotic solvents, such as N, N-dimethylformamide and acetonitrile, to promote their dissolution in electrolytes and sustain high TOFs.^[6] The integrated electrolytic cells in practice requires aqueous solutions, where few homogeneous catalysts exhibit sufficient activity or selectivity.^[6b, 7] Another issue that homogeneous catalysts face is the difficulty to be separated from electrolytes for recycle or products extraction purpose, and they are incompatible with flow cells.^[8] Heterogeneous catalysts generally exhibit the opposite characteristics. Such catalysts are robust and operative in aqueous solutions, while it is not easy to understand catalytic mechanism and tune the activity at molecular levels due to the surface structure complexity.^[9] Immobilizing homogeneous catalysts onto conductive substrates combines the advantages of molecular catalysis with the convenience of heterogeneous catalysis in aqueous solutions, and represents a promising approach to overcome these drawbacks.

Various studies have been carried out to immobilize homogeneous catalysts onto conductive substrates, including covalent or noncovalent linking,^[6b, 10] assembly into metal or covalent organic frameworks,^[11] polymerization^[12] and directly casting water-insoluble molecules^[13]. Among these studies, complexes of metal phthalocyanines and porphyrins represent an important class of CO₂RR molecular catalysts. Their planar structures are suitable for surface attachment with substrates to form monolayers with the axial sites of metal centers providing the active sites.^[8b, 14] Except for the selection of appropriate active

sites, in heterogeneous states, the electrocatalysis on complexes also relies on the electron communication between the metal centers and substrates, which is closely related to the structures of linkages between the metal centers and solids. The molecular length, rigidities and π -conjugation degree of linkages determine the distance and pathways for electron transfer.^[15] Poorly chosen linkages might obstruct such electron communications, which makes the metal sites electro inactive that cannot serve as the active sites.^[11a]

Based on the aforementioned considerations, we developed a heterogeneous CO₂RR electrocatalyst that is operative in aqueous solution by immobilizing planar Co(II)-2,3-naphthalocyanine complexes (NapCo) on doped graphene based matrices and investigated the linkage effects. Graphene is a suitable substrate because it has high conductivity, stability under reductive environments and good reactivity to allow versatile linkages to connect with molecules.^[16] NapCo has a high π -conjugation degree to allow π - π stacking with graphene. Besides, the axial coordination for NapCo provides another driving force for the immobilization, and such an interaction has shown the potential to intrinsically improve the CO₂RR activity/selectivity of the immobilized Co sites.^[17] We found that graphitic sulfoxide and carboxyl dopants of graphene served as major linking sites for NapCo through forming axial Co-O coordination. Such configurations resulted in the active and molecular Co sites for CO₂RR. Additionally, the sulfoxide dopants greatly promoted the electron communication between the immobilized Co sites and graphene comparing to the carboxyl based linking site. The sulfoxide-NapCo moiety derived a high selectivity of CO₂-to-CO conversion (97% at -0.8 V) and increased the TOF of Co sites by ~3 times comparing to that of carboxyl-NapCo moiety. The pristine NapCo in the absence of graphene supports did not have redox response and was thus electrochemically inactive for CO₂RR.

Results and Discussion

Heterogenization of molecular Co sites. In a typical synthetic process, GO aqueous solution (~1 mg mL⁻¹) was modified with thiourea under hydrothermal conditions, forming S/N/O heteroatoms doped graphene (SNG). The SNG was mixed with NapCo in DMF at 80 °C to derive a heterogeneous catalyst (denoted as NapCo@SNG). The complexes can be immobilized onto SNG through π - π stacking. The heteroatoms doped in graphene contained extra electrons comparing to the neighboring carbon atoms and they were proposed to serve as another type of linking site that can tune the coordination

configuration of NapCo on graphene (Figure 1a). Thus, for comparison, in the control experiments, O and N/O doped graphene (OG and NG) were synthesized from GO using the similar hydrothermal method. NapCo was immobilized onto the OG and NG to form NapCo@OG and NapCo@NG following the same procedures as the synthesis of NapCo@SNG (details were provided in the experiments of supporting information, SI).

The scanning and transmission electron microscopic (SEM/TEM) images (Figure 1b, S1) revealed the two-dimensional structure of NapCo@SNG with substantial scrolls and wrinkles, which are the characteristics of graphene. On these graphene layers, we did not observe any nanoparticles of metallic Co or Co oxides, indicating that NapCo was not decomposed under the synthesis conditions. In X-ray photoelectron spectroscopy (XPS, Figure 1c) surveys, the NapCo@SNG showed two main peaks at 779.8 eV and 795.4 eV with an intensity ratio of 2:1, assigning to the Co $2p_{3/2}$ and $2p_{1/2}$ core levels, respectively. Meanwhile, the immobilization of Co sites generated a strong N $1s$ peak centered at 397.4 eV assigning to the Nap ligands (Figure 1c inset). The NapCo@SNG was probed by aberration-corrected high-angle annular dark-field scanning TEM (HAADF-STEM, Figure 1d and S2). Substantial bright spots (sizes less than 0.15 nm) corresponding to the molecular Co sites were uniformly distributed over the graphene layers. The ultraviolet-visible (UV-vis, Figure 1d, S3a) spectra showed that two absorbance bands of NapCo at 270 nm and 364 nm, corresponding to the metal-to-ligand charge transition (MLCT) and $d-d$ transition, respectively. The latter transition on NapCo@SNG exhibited a red shift (from 364 nm to 371 nm) comparing to that of pristine NapCo, which might reflect that the charge transfer occurred between the Co sites and SNG. Such a red shift was also observed upon immobilizing NapCo onto OG and NG (Figure S3b, c).

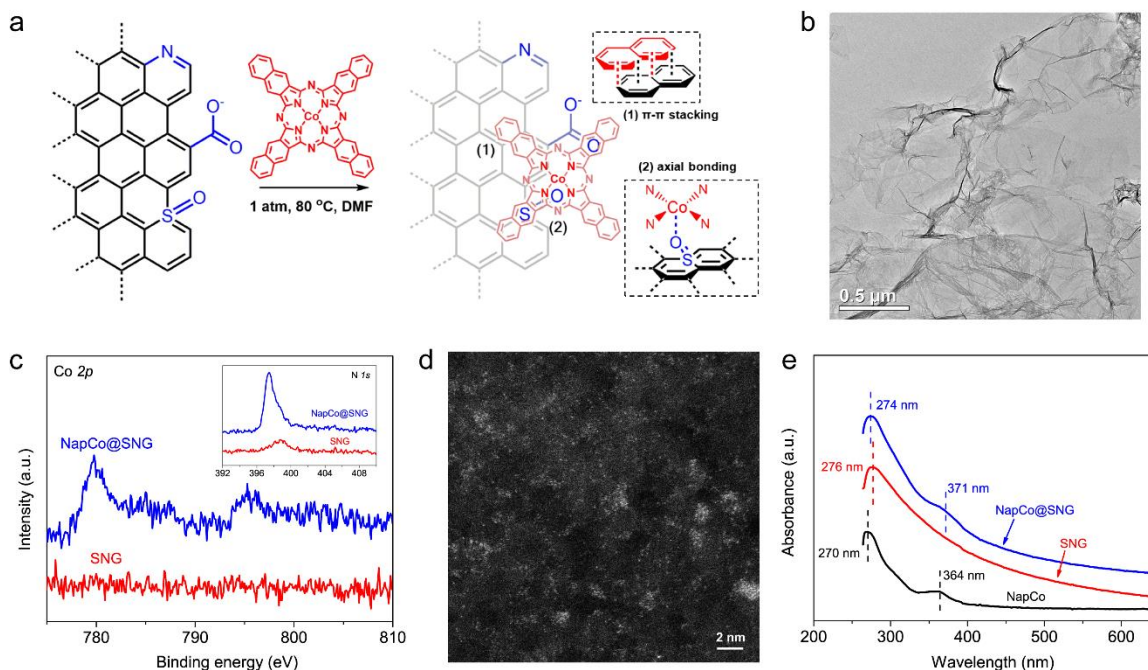


Figure 1. (a) Heterogenization of NapCo onto doped graphene through π - π stacking and coordination with heteroatoms. (b) A typical bright-field TEM image of NapCo@SNG. (c) XPS surveys of Co 2p core electron levels of SNG and NapCo@SNG, respectively. Inset shows the N 1s core electron levels of SNG and NapCo@SNG. (d) HAADF-STEM images of NapCo@SNG. The Co atoms are indicated by the bright spots. (e) UV-vis spectra of NapCo before and after immobilizing onto SNG.

Binding between molecular Co sites and graphene. The heterogenized Co sites were investigated by X-ray absorption spectroscopy (XAS). In the normalized X-ray absorption near edge spectra (XANES, Figure 2a), the absorption edge of NapCo@SNG clearly shifted to lower energy than that of NapCo (shift by ~ 1 eV for the energy at edge-jump of 0.5), indicating a strong electronic interaction between NapCo and SNG. In the Fourier-transformed extended X-ray absorption fine structure spectra (FT-EXAFS, Figure 2b), centering on the first shells, the peak position of NapCo occurred at R value of 1.4 \AA for the Co-N bonds. For NapCo@SNG, this Co-N peak slightly shifted to 1.35 \AA . Notably, a shoulder peak appeared near ~ 1.7 \AA . Such a variation suggested that the coordination shell of Co sites was tuned by SNG.

For the XAS data of NapCo@OG/NG (Figure 2c), it was also observed that the absorption edges of Co sites shifted to lower energies with the immobilization. However,

in the FT-EXAFS data (Figure 2d), both the control samples exhibited the distinct signals on the first shells of Co sites from NapCo@SNG, and we did not observe the shoulder signal as the one occurred in the FT-EXAFS data of NapCo@SNG. Apparently, the immobilization of NapCo on the doped graphenes were not simply driven by π - π stacking, but also was determined by possible interaction between Co sites and the different dopants of graphene. The S dopants should lead to a distinct binding configuration of NapCo on graphene comparing to the O and N dopants. By CHNS elemental analysis combining with inductively coupled plasma mass spectrometric (ICP) measurements, we estimated the atomic ratios of those dopants (i.e., S, N and O atoms) in different graphenes to the immobilized Co sites (Table S2, S3), showing that those dopants were sufficient as the major linking sites for NapCo.

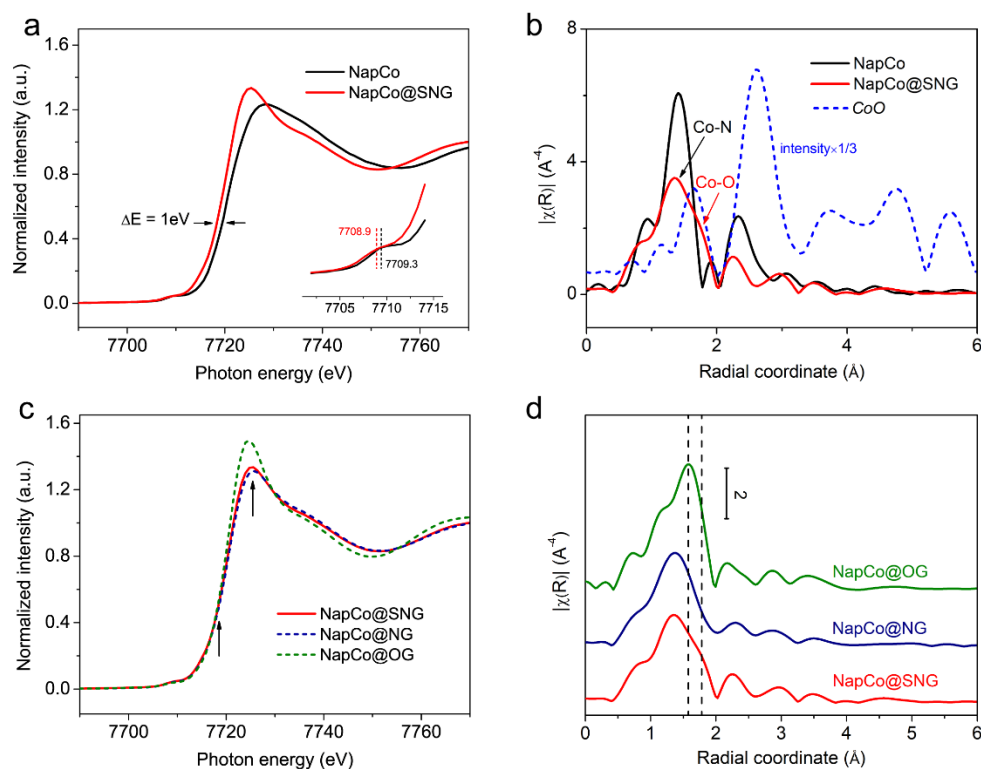


Figure 2. (a) Co K-edge XANES data of NapCo@SNG and NapCo. (b) FT-EXAFS data of NapCo@SNG, NapCo and a CoO reference without phase correction. (c) Co K-edge XANES data of NapCo@SNG, NapCo@NG and NapCo@OG, (d) their FT-EXAFS data without phase correction.

In the XPS surveys (Figure S4), SNG showed the distinct S 2p spectrum with two bands centering at 163 eV and 167.2 eV, which were assigned to the doped structures of carbon

sulfides and oxidized sulfurs, respectively.^[18] The N *1s* band of SNG centered at 398.8 eV for pyridine or/and pyrrole structures as observed in NG.^[19] The O *1s* bands indicated that the O dopants were mainly in the forms of carboxyl (530.5 eV) and hydroxyl (532.5 eV) structures, which were similar to those in OG and NG.^[20] The binding states of NapCo on these dopants of graphene were investigated by density functional theory (DFT) calculations. It was found that the pyridinic sulfoxide (SO) or graphitic SO of oxidized sulfurs were very efficient binding sites to immobilize NapCo through Co-O bonding along the axial position of Co site, which was revealed by the clear charge transfer occurred between the Co sites and SO dopants (Figure 3a, b and S5). Because of such a clear chemical bonding nature, the axial Co-O bonds should be more significant to determine the immobilization of NapCo comparing to pure π - π stacking, which is van der waals interaction. The optimized axial bond lengths for these two cases were 2.09 Å and 2.08 Å, respectively, which were consistent with the Co-O distance of 2.08 ± 0.02 Å fitted by the EXAFS data of NapCo@SNG. The oxidized sulfurs might involve other structures such as sulfonate (SO₂) and sulfonic acid (SO₃H). These dopants can also form the axial Co-O bonds with NapCo. The calculated bond lengths increased to 2.21 Å and 2.25 Å, respectively, excluding the possible presence of such groups (Figure 3c, S6a-d). Additionally, our calculation also showed that there was no electronic interaction between NapCo and the carbon sulfides of graphene (Figure S6e, f). Therefore, for NapCo@SNG, we suggested that pyridinic or graphitic SO dopants were the main binding sites for the immobilization of NapCo.

Both pyridinic and pyrrolic N dopants in NG were not the efficient binding sites to NapCo as they only exhibited van der waals interaction with the Co sites (Figure S7). In contrast, carboxyl (COO) structure of O dopants in NG and OG was identified to be a binding site for NapCo in the absence of the oxidized sulfur dopants. The axial Co-O bond formed between COO and NapCo as indicated by the clear charge transfer between the Co and COO dopant (Figure 3d, S8). The optimized bond length was 2.00 Å, which was close to the Co-O distance of 2.08 ± 0.02 Å fitted by the EXAFS data of NapCo@OG. Although a hydroxyl oxygen of graphene could also form the axial Co-O bond with NapCo, the charge transfer was less significant than that observed on the COO site and the Co-O bond length prolonged to be 2.18 Å (Figure S9).

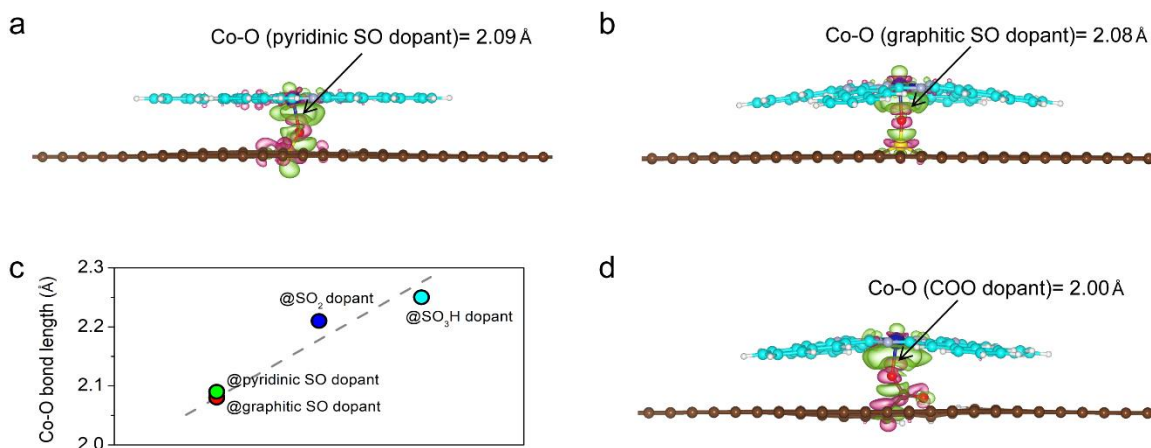


Figure 3. Charge density difference of NapCo immobilized on pyridinic SO (a) and graphitic SO (b) dopants of graphene. (c) The Co-O bond lengths for NapCo on SO, SO₂ and SO₃H dopants of graphene. (d) Charge density difference of NapCo on a COO dopant of graphene. The charge accumulation regions were colored in pink and charge depletion regions were colored in green. The charge density difference was obtained via subtracting the total charge densities of adsorbed NapCo and graphene from that of NapCo@graphene. Iso-surface level was set to $\pm 0.001 e/\text{bohr}^3$. The brown, cyan, white, yellow, red, blue and light blue spheres represent C atoms of graphene, C atoms of NapCo, H, S, O, Co and N atoms, respectively.

Electrochemical measurements. We next investigated the redox of Co sites by cyclic voltammetry (CV, Figure S10a-c), after depositing NapCo@SNG on a planar glassy carbon electrode (GCE). The immobilized Co sites were redox active in 0.1 M KHCO₃ as indicated by a pair of redox peaks ($E_{1/2} \sim -0$ V) assigning to Co^{2+/1+} couples^[21] (all potentials were quoted against the reversible hydrogen electrode, RHE, unless stated otherwise). The peak currents are linearly correlated with the scan rates to indicate the immobilized states of Co sites on graphene. The rate constant (k_s) of the redox was calculated by the Laviron's equation to be 27.8 s⁻¹, which was comparable to those of very redox-active monolayers on electrodes.^[15a, 22] We took the advantage of the insolubility of NapCo in water and directly cast them onto GCE. Even by using differential pulse voltammetry (DPV) measurement, the redox of Co sites was not observed in the same potential range (Figure S10d) due to the low conductivity of bulk NapCo. These results suggested that the redox of molecular Co sites was realized through the support of SNG, and the electron transfer between the

molecular Co sites and SNG was rapid.

The CO₂RR electrocatalysis on NapCo@SNG was conducted in 0.1 M KHCO₃ with continuous purging of CO₂. CO₂RR currents were observed with an onset potential of -0.4 V (Figure 4a). The products were analyzed by in-line gas chromatography (GC) and high-performance liquid chromatography (HPLC). H₂ and CO were the only products and other possible products (hydrocarbons or acids) were not detected. Ranging the potentials from -0.4 V to -0.8 V, the Faradic efficiency for CO production (FES_{CO}) gradually increased from 67.5% to 97%. The FES_{CO} are superior to most heterogenous molecular Co catalysts and metallic metal catalysts reported recently (Table S4). The CO₂RR activity of NapCo@NG and NapCo@OG was studied for comparison. Both the control samples displayed slightly lower CO selectivity at all potentials and lower stability in continuous running (Figure 4b, c). Notably, pristine NapCo in the absence of graphene afforded low FES_{CO} (20%-25%) and almost negligible currents as the Co sites were not redox active in the bulk structure and did not serve as the efficient electrochemical sites to catalyze CO₂RR (Figure S11). The FES_{CO} of pristine SNG, NG and OG were all much lower than the ones collected in the presence of NapCo and their CO₂RR currents were trivial (Figure S12, S13). Additionally, formate was detected for CO₂RR on SNG and NG. This product was not observed after NapCo was immobilized onto graphene. These results supported that the Co sites on graphene were the main active sites responsible for CO₂RR and the contribution from graphene was insignificant. The TOFs of Co sites, as an indication of specific activity, were thus calculated according to the following equation (1),

$$\text{TOF} = (J_{co} \times A) / (2 \times F \times m) \quad (1)$$

where J_{co} is the CO₂RR current density, A is the geometrical surface area of the electrode, F is the Faraday constant, and m is the amount of Co sites on the doped graphene. The m was determined by ICP (Table S2). Assuming that all the Co sites on the electrodes were involved in CO₂RR, NapCo@SNG afforded higher TOFs than the ones achieved on NapCo@OG (e.g. at -0.735 V, 0.45 s⁻¹ vs 0.16 s⁻¹, Figure 4d). The TOFs of NapCo@NG were also relatively low, in agreement with the DFT results that N dopants had the limited ability to tune the binding configurations of Co sites on the doped graphene (Figure S7).

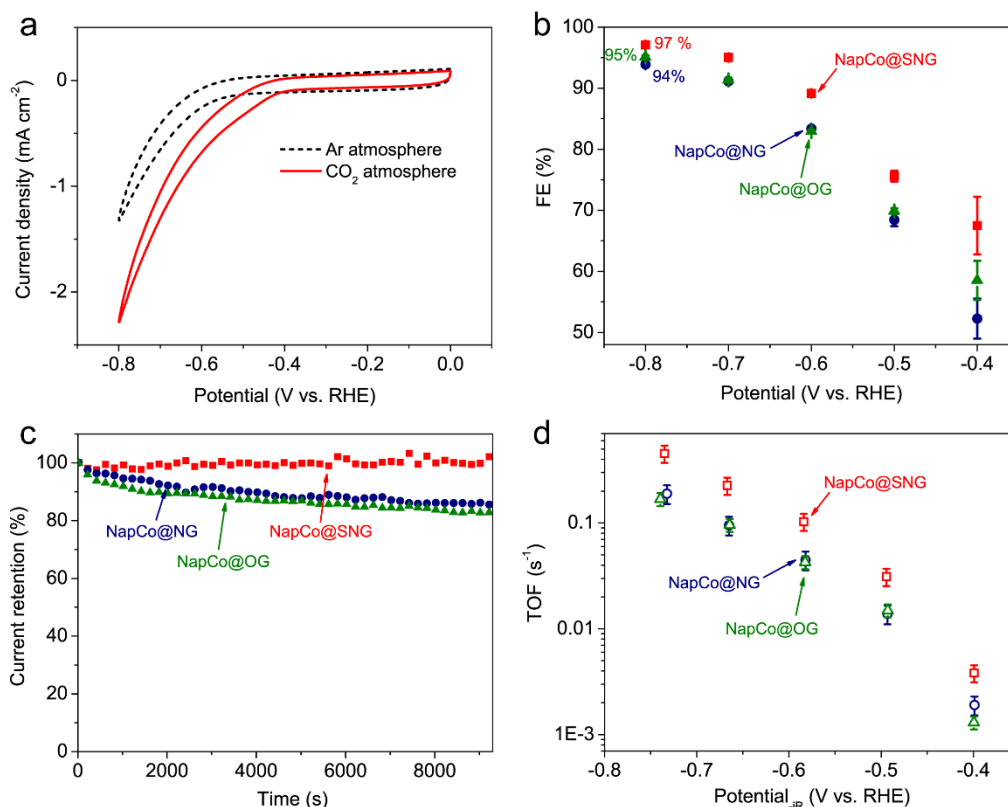


Figure 4. (a) CVs of NapCo@SNG in Ar- and CO₂-saturated 0.1 M KHCO₃. (b) FE_{CO} of CO₂RR on NapCo@SNG/NG/OG, CO₂-saturated 0.1 M KHCO₃. (c) The corresponding chronoamperometric curves of NapCo@SNG, NapCo@NG and NapCo@OG at -0.8 V. (d) TOFs of Co sites@SNG/NG/OG for CO production.

Insights into electrocatalysis of Co sites on S-doped graphene. To verify that the S dopants are indeed the key to promote the specific activity of the immobilized Co sites, we further synthesized two S/O-doped graphenes by modifying GO with NaSH or CS₂ (denoted as SG-1 and SG-2). SG-1 and SG-2 have an S content of ~1.7% and ~5.7%, respectively (~9.3% for SNG, Figure S14). NapCo@SG-1/-2 was then prepared and tested as CO₂RR electrocatalysts (details were provided in the experiments of SI). For NapCo@SG-1/-2, UV-vis spectra showed the characteristic *d-d* transition of NapCo at 372-374 nm (Figure S15). XPS surveys presented the clear Co and N signals from NapCo (Figure S16). The CO₂RR measurements showed that NapCo@SG-1/-2 were selective and durable for CO production (Figure S17, S18). The activities of pristine SG-1/-2 was insignificant compared to the Co sites-enabled CO₂RR (Figure S19). By normalizing the CO₂RR currents with the Co amounts, NapCo@SG-1/-2 afforded similar TOFs as

NapCo@SNG ($0.5 \text{ s}^{-1}/0.4 \text{ s}^{-1}$ at -0.735 V , Figure 5a).

XPS surveys showed that the S dopants of SG-1/-2 both contained the oxidized sulfur structures (Figure 5b). The normalized XANES data of NapCo@SG-1/-2 (Figure S20) were very close to those of NapCo@SNG. In the EXAFS analysis (Figure 5c), the first shells of Co sites in NapCo@SG-1/-2 also exhibited the shoulder signals for R value near 1.7 \AA as observed in the EXAFS data of NapCo@SNG to derive a fitted Co-O distance of $2.06 \pm 0.02 \text{ \AA}$ and $2.08 \pm 0.02 \text{ \AA}$, respectively. These results suggested that the binding configurations of NapCo on SG-1/-2 were very close to that on SNG (Figure 3d), and thus the SO dopants of graphene should serve as the main binding sites to NapCo. We found that the axial coordination of SO dopants tuned the intrinsic CO₂RR activity of NapCo. The DFT calculation confirmed that the Co sites were the active sites of CO₂RR. The protonation of CO₂ to *COOH determines the overpotentials (Figure 5d). For NapCo on a pyridinic SO dopant, the Co site afforded a relatively large theoretical CO₂RR overpotential of 0.42 V. In contrast, NapCo on graphitic SO and COO dopants of graphene are more active. The theoretical CO₂RR overpotentials decreased to 0.27 V and 0.29 V, respectively, which are not very far from the experimentally observed value in the CO₂RR measurements of NapCo@SNG and NapCo@OG (their onset potentials were $\sim -0.4 \text{ V}$, Figure S13). Indeed, calculation shows that these two Co sites were relatively more active than the Co sites on the other possibly involved dopants of graphene (Figure 5e). Therefore, we considered that the Co sites with axial coordination of the graphitic SO and COO dopants of graphene were the main configurations in NapCo@SNG and NapCo@OG, respectively, to dominate the electrocatalysis of CO₂RR. Our DFT calculation combining with electrochemical analyses are also consistent with the previous results that the axial coordination can be prominent to determine the CO₂RR activity of the molecular Co sites in the heterogeneous catalysis.^[17]

Although DFT calculation shows that the NapCo on graphitic SO and COO dopants afforded similar intrinsic activity, quite different TOFs were observed experimentally on NapCo@SNG and NapCo@OG. We therefore investigated the redox responses of the immobilized Co sites by DPVs to verify if the electron communication between NapCo and the different doped graphenes was efficient. The redox potentials of Co sites on the different doped graphenes all occurred near 0 V. While in the presence of S dopants, the DPV currents of the immobilized Co sites on graphene were clearly improved (Figure 5f, S21). It was suspected that whether such different redox responses were simply determined

by the conductivity of graphene tuned by the dopants. We used ferrocyanide/ferricyanide couple ($\text{Fe}(\text{CN})_6^{4-/3-}$) to probe the electron transport ability of the doped graphene. Although this probe at certain levels might be sensitive to the surface compositions of carbon electrodes, it is generally accepted that the coordination shell of $\text{Fe}(\text{CN})_6^{4-/3-}$ remained intact during the redox process to have very weak interaction with the different dopants in graphene. The electron transfer proceeds through the mechanism of outer sphere electron transfer to reflect the bulk conductivity of graphene.^[23] The CVs showed that the redox currents of $\text{Fe}(\text{CN})_6^{4-/3-}$ on the different doped graphenes were close (Figure S22a). The redox kinetics of $\text{Fe}(\text{CN})_6^{4-/3-}$ were analyzed by the Laviron's method.^[22] It showed that the k_s were all near 1 s^{-1} (Figure S22b, c). Therefore, in our doping levels, the different dopants have very weak impacts on the electron transport ability of graphene skeletons. For the immobilized NapCo, the redox of Co sites could be closely related to their binding configurations with the dopants of graphene. Therefore, the different doped graphenes were electrochemically probed by CoSO_4/KCl solutions. Under this condition, Co ions lack strongly-adsorbed ligands. They tend to interact more easily with the dopants of graphene comparing to $\text{Fe}(\text{CN})_6^{4-/3-}$, such that the redox currents of CoSO_4/KCl probe the electron transfer ability of those different dopants of graphene. It showed that the redox responses of Co ions on graphene with the S dopants (SG-1/-2/SNG) were all higher than those on OG (Figure S23). These results well supported that through the SO dopants as the efficient binding sites of Co sites, it resulted in the improved electron communication between NapCo and graphene, making the immobilized Co sites electro active as the reacting sites to enable the electron transfer in CO_2RR .

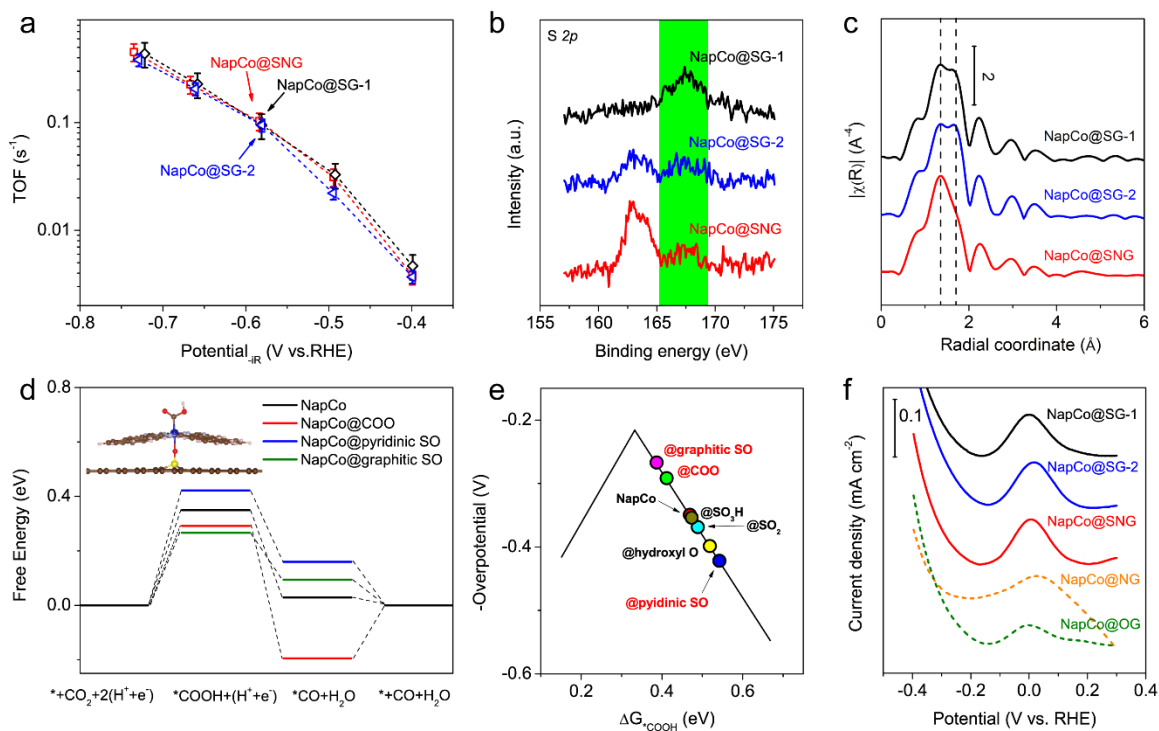


Figure 5. (a) TOFs of Co sites for CO production at SNG, SG-1 and SG-2. (b) Comparison of XPS S 2p core levels of NapCo@SNG, NapCo@SG-1 and NapCo@SG-2. (c) The corresponding FT-EXAFS data at Co-K edge without phase correction. (d) Free energy diagrams of CO₂RR on free-standing NapCo and NapCo bonded with COO, pyridinic SO and graphitic SO doped graphene. Inset shows the formation of *COOH on Co sites as the rate-limiting step of CO₂RR. (e) Calculated overpotentials of CO₂RR on NapCo bonded with various dopants of graphene as a function of ΔG_{COOH}^* . (f) DPVs of NapCo@SG-1/SG-2/SNG/NG/OG collected in Ar saturated 0.1 M KHCO₃. Amplitude: 50 mV; Pulse width: 0.05 s; Sampling width: 0.0167 s; Pulse period: 0.5 s.

Conclusion

In summary, we investigated the immobilization of planar complexes, NapCo, onto doped graphene matrices at a mild condition toward the heterogeneous electrocatalysis of CO₂RR. Pristine NapCo on the electrode did not exhibit redox responses with applying potentials that was not electrochemically active to catalyze CO₂RR. The redox of Co sites was enabled with immobilizing NapCo onto the doped graphene, and the k_s of redox was up to 27.8 s⁻¹ to indicate the rapid electron communication between the Co sites and graphene. By both experimental and theoretical investigations, we suggested that graphitic

SO and COO dopants of graphene were the efficient binding sites to NapCo through the axial coordination with Co sites. Such heterogenized Co configurations served as the main active sites to selective reduction of CO₂ into CO with Faradic efficiency up to 97%. The SO dopants could further facilitate the electron communication between NapCo and graphene resulted in an enhancement of CO₂RR activity. The TOF of Co sites were increased by ~3 times on S-doped graphene comparing to the one on O-doped graphene. Our results demonstrated a novel and easy strategy of immobilizing molecular active sites to form heterogeneous catalyst for CO₂RR.

Acknowledgements

This project was funded by the National Research Foundation (NRF), Prime Minister's Office, Singapore, under its Campus for Research Excellence and Technological Enterprise (CREATE) program. We acknowledge financial support from the academic research fund AcRF tier 1 (M4011784 RG6/17 and M4012076 RG118/18), Ministry of Education, Singapore and Startup grant (M4081887), College of Engineering, Nanyang Technological University. This research used resources of the Tender Energy Absorption Spectroscopy Beamline of the National Synchrotron Light Source II, a U.S. Department of Energy (DOE) Office of Science User Facility operated for the DOE Office of Science by Brookhaven National Laboratory under Contract No. DE-SC0012704.

Author Contribution

#These authors equally contribute to the work.

References

- [1] a) Y. Hori, in *Modern Aspects of Electrochemistry* (Eds.: C. G. Vayenas, R. E. White, M. E. Gamboa-Aldeco), Springer New York, New York, NY, **2008**, pp. 89-189; b) G. Centi, S. Perathoner, *Catal. Today* **2009**, *148*, 191-205; c) M. Mikkelsen, M. Jorgensen, F. C. Krebs, *Energy Environ. Sci.* **2010**, *3*, 43-81; d) J. Qiao, Y. Liu, F. Hong, J. Zhang, *Chem. Soc. Rev.* **2014**, *43*, 631-675.
- [2] a) A. Seifitokaldani, C. M. Gabardo, T. Burdyny, C.-T. Dinh, J. P. Edwards, M. G. Kibria, O. S. Bushuyev, S. O. Kelley, D. Sinton, E. H. Sargent, *J. Am. Chem. Soc.* **2018**, *140*, 3833-3837; b) A. J. Garza, A. T. Bell, M. Head-Gordon, *ACS Catal.* **2018**, *8*, 1490-1499; c) Y. Zheng, A. Vasileff, X. Zhou, Y. Jiao, M. Jaroniec, S.-Z. Qiao, *J. Am. Chem. Soc.* **2019**, *141*, 7646-7659.
- [3] a) M. Jouny, W. Luc, F. Jiao, *Ind. Eng. Chem. Res.* **2018**, *57*, 2165-2177; b) C. K.

- Rofer-DePoorter, *Chem. Rev.* **1981**, *81*, 447-474.
- [4] a) T. Fukushima, W. Drisdell, J. Yano, Y. Surendranath, *J. Am. Chem. Soc.* **2015**, *137*, 10926-10929; b) C. Costentin, S. Drouet, M. Robert, J.-M. Savéant, *Science* **2012**, *338*, 90-94; c) S. Bang, Y.-M. Lee, S. Hong, K.-B. Cho, Y. Nishida, M. S. Seo, R. Sarangi, S. Fukuzumi, W. Nam, *Nat. Chem.* **2014**, *6*, 934.
- [5] a) T. E. Rosser, E. Reisner, *ACS Catal.* **2017**, *7*, 3131-3141; b) Z. Chen, J. J. Concepcion, M. K. Brennaman, P. Kang, M. R. Norris, P. G. Hoertz, T. J. Meyer, *Proc. Natl. Acad. Sci.* **2012**, *109*, 15606-15611; c) C. Riplinger, M. D. Sampson, A. M. Ritzmann, C. P. Kubiak, E. A. Carter, *J. Am. Chem. Soc.* **2014**, *136*, 16285-16298.
- [6] a) I. Bhugun, D. Lexa, J.-M. Savéant, *J. Am. Chem. Soc.* **1996**, *118*, 1769-1776; b) A. Maurin, M. Robert, *J. Am. Chem. Soc.* **2016**, *138*, 2492-2495.
- [7] a) H. Takeda, C. Cometto, O. Ishitani, M. Robert, *ACS Catal.* **2017**, *7*, 70-88; b) S. A. Yao, R. E. Ruther, L. Zhang, R. A. Franking, R. J. Hamers, J. F. Berry, *J. Am. Chem. Soc.* **2012**, *134*, 15632-15635.
- [8] a) D. J. Cole-Hamilton, *Science* **2003**, *299*, 1702-1706; b) S. Berner, S. Biela, G. Ledung, A. Gogoll, J.-E. Bäckvall, C. Puglia, S. Oscarsson, *J. Catal.* **2006**, *244*, 86-91.
- [9] a) Q. Lu, F. Jiao, *Nano Energy* **2016**, *29*, 439-456; b) Z. Sun, T. Ma, H. Tao, Q. Fan, B. Han, *Chem* **2017**, *3*, 560-587; c) N. D. Schley, J. D. Blakemore, N. K. Subbaiyan, C. D. Incarvito, F. D'Souza, R. H. Crabtree, G. W. Brudvig, *J. Am. Chem. Soc.* **2011**, *133*, 10473-10481.
- [10] a) M. Schreier, J. Luo, P. Gao, T. Moehl, M. T. Mayer, M. Grätzel, *J. Am. Chem. Soc.* **2016**, *138*, 1938-1946; b) G. Sahara, R. Abe, M. Higashi, T. Morikawa, K. Maeda, Y. Ueda, O. Ishitani, *Chem. Commun.* **2015**, *51*, 10722-10725; c) J. D. Blakemore, A. Gupta, J. J. Warren, B. S. Brunschwig, H. B. Gray, *J. Am. Chem. Soc.* **2013**, *135*, 18288-18291; d) J. Wang, X. Ge, Z. Liu, L. Thia, Y. Yan, W. Xiao, X. Wang, *J. Am. Chem. Soc.* **2017**, *139*, 1878-1884; e) J. Wang, L. Gan, Q. Zhang, V. Reddu, Y. Peng, Z. Liu, X. Xia, C. Wang, X. Wang, *Adv. Energy Mater.* **2019**, *9*, 1803151; f) M. N. Jackson, S. Oh, C. J. Kaminsky, S. B. Chu, G. Zhang, J. T. Miller, Y. Surendranath, *J. Am. Chem. Soc.* **2018**, *140*, 1004-1010; g) X. Zhang, Z. Wu, X. Zhang, L. Li, Y. Li, H. Xu, X. Li, X. Yu, Z. Zhang, Y. Liang, H. Wang, *Nat. Commun.* **2017**, *8*, 14675; h) V. Artero, *Nat. Energy* **2017**, *2*, 17131; i) C. M. Lieber, N. S. Lewis, *J. Am. Chem. Soc.* **1984**, *106*, 5033-5034.
- [11] a) S. Lin, C. S. Diercks, Y.-B. Zhang, N. Kornienko, E. M. Nichols, Y. Zhao, A. R. Paris, D. Kim, P. Yang, O. M. Yaghi, C. J. Chang, *Science* **2015**; b) N. Kornienko, Y. Zhao, C. S. Kley, C. Zhu, D. Kim, S. Lin, C. J. Chang, O. M. Yaghi, P. Yang, *J. Am. Chem. Soc.* **2015**, *137*, 14129-14135.
- [12] S. Sato, T. Arai, T. Morikawa, K. Uemura, T. M. Suzuki, H. Tanaka, T. Kajino, *J. Am. Chem. Soc.* **2011**, *133*, 15240-15243.
- [13] a) Z. Weng, J. Jiang, Y. Wu, Z. Wu, X. Guo, K. L. Materna, W. Liu, V. S. Batista,

- G. W. Brudvig, H. Wang, *J. Am. Chem. Soc.* **2016**, *138*, 8076-8079; b) T. Yoshida, K. Kamato, M. Tsukamoto, T. Iida, D. Schlettwein, D. Wöhrle, M. Kaneko, *J. Electroanal. Chem.* **1995**, *385*, 209-225; c) T. Abe, T. Yoshida, S. Tokita, F. Taguchi, H. Imaya, M. Kaneko, *J. Electroanal. Chem.* **1996**, *412*, 125-132; d) M. Zhu, R. Ye, K. Jin, N. Lazouski, K. Manthiram, *ACS Energy Lett.* **2018**, *3*, 1381-1386.
- [14] W. Hieringer, K. Flechtner, A. Kretschmann, K. Seufert, W. Auwärter, J. V. Barth, A. Görling, H.-P. Steinrück, J. M. Gottfried, *J. Am. Chem. Soc.* **2011**, *133*, 6206-6222.
- [15] a) A. L. Eckermann, D. J. Feld, J. A. Shaw, T. J. Meade, *Coord. Chem. Rev.* **2010**, *254*, 1769-1802; b) M. Gilbert Gatty, A. Kahnt, L. J. Esdaile, M. Hutin, H. L. Anderson, B. Albinsson, *J. Phys. Chem. B* **2015**, *119*, 7598-7611.
- [16] a) R. L. McCreery, *Chem. Rev.* **2008**, *108*, 2646-2687; b) C. Backes, F. Hauke, A. Hirsch, *Adv. Mater.* **2011**, *23*, 2588-2601.
- [17] a) W. W. Kramer, C. C. L. McCrory, *Chem. Sci.* **2016**, *7*, 2506-2515; b) Y. Liu, C. C. L. McCrory, *Nat. Commun.* **2019**, *10*, 1683.
- [18] B. J. Lindberg, K. Hamrin, G. Johansson, U. Gelius, A. Fahlman, C. Nordling, K. Siegbahn, *Phys. Scr.* **1970**, *1*, 286.
- [19] Y.-F. Lu, S.-T. Lo, J.-C. Lin, W. Zhang, J.-Y. Lu, F.-H. Liu, C.-M. Tseng, Y.-H. Lee, C.-T. Liang, L.-J. Li, *ACS Nano* **2013**, *7*, 6522-6532.
- [20] R. Arrigo, M. Hävecker, S. Wrabetz, R. Blume, M. Lerch, J. McGregor, E. P. J. Parrott, J. A. Zeitler, L. F. Gladden, A. Knop-Gericke, R. Schlögl, D. S. Su, *J. Am. Chem. Soc.* **2010**, *132*, 9616-9630.
- [21] a) M. T. de Groot, M. T. M. Koper, *Phys. Chem. Chem. Phys.* **2008**, *10*, 1023-1031; b) A. van der Putten, A. Elzing, W. Visscher, E. Barendrecht, *J. Electroanal. Chem.* **1987**, *221*, 95-104.
- [22] E. Laviron, *J. Electroanal. Chem.* **1979**, *100*, 263-270.
- [23] a) L. M. Torres, A. F. Gil, L. Galicia, I. González, *J. Chem. Edu.* **1996**, *73*, 808; b) I. Duo, A. Fujishima, C. Comninellis, *Electrochem. Commun.* **2003**, *5*, 695-700; c) L. Xiong, C. Batchelor-McAuley, K. R. Ward, C. Downing, R. S. Hartshorne, N. S. Lawrence, R. G. Compton, *J. Electroanal. Chem.* **2011**, *661*, 144-149.